Transit times in turbulent flows

H. L. Pécseli[1] and J. Trulsen[2]
[1]*Department of Physics, University of Oslo, Box 1048 Blindern, N-0316 Oslo, Norway*
[2]*Institute of Theoretical Astrophysics, University of Oslo, Box 1029 Blindern, N-0315 Oslo, Norway*
(Received 27 August 2009; published 14 April 2010)

Statistics of the motion of passively convected point particles in turbulent flows are studied. The database used is obtained by direct numerical solution of the Navier-Stokes equation. We estimate the probability distribution of the transit times of such particles through reference volumes with given forms and sizes. A selected position within the reference volume is moving with the local flow velocity, thus determining the motion of the entire surface. The transit time is defined as the interval between entrance and exit times of surrounding particles convected through the volume by the turbulent motions. Spherical as well as hemispherical surfaces are studied. Scale sizes in the inertial as well as in the viscous subranges of the turbulence are considered. Simple, and seemingly universal, scaling laws are obtained for the probability density of the transit times in terms of the basic properties of the turbulent flow and the geometry. In the present formulation, the results of the analysis are relevant for chemical reactions, but also for understanding details of the feeding rate of micro-organisms in turbulent waters, for instance.

DOI: 10.1103/PhysRevE.81.046310 PACS number(s): 47.27.E−, 47.27.tb

I. INTRODUCTION

One of the basic problems associated with dispersal of particles by turbulent flows concerns the relative separation of two particles. In the present study, we consider a related problem, by analyzing the transit time (or passage time [1]) of a particle through a reference volume moving with the flow. We thus take a reference volume with constant shape (for instance, a sphere), and let a reference point associated with the volume (the center of the sphere, for instance) be moving with the local flow. The transit time is defined as the interval between the entrance and first exit times of surrounding particles passing through the reference volume. The analysis is carried out by use of two large databases obtained by numerical solutions of the Navier-Stokes equation [2,3]. with parameters listed in Table I. We consider spherical and also hemispherical reference volumes. Given the shape of the reference volumes, the scaling laws found seem to have general validity.

The relevance of this problem, for instance, for chemical reactions has been pointed out elsewhere [1]. We find another interesting application of the present problem in noting that turbulent mixing seem to be important for the feeding processes of zoo plankton in the oceans [4], where, in particular, models for the encounter rate in turbulent environments have been proposed before [5–7]. The transit time, as defined in this study, is the time available for interaction between the transiting particle and the reference particle. The two particles can, for instance, represent prey and predator. The interaction time defined before then represents the time available for a small predator to capture its prey; this time is an important parameter for modeling the process [8,9]. Also, other relevant problems can be found [10]. Analytically solvable models for the problem have also been proposed [1], including results for the transit time probability densities.

We have analyzed parts of this problem previously [7,11] by using data from a laboratory experiment, where turbulence with reproducible parameters could be generated by two moving grids [12]. The scatter in these results was significant because of the uncertainties involved, the estimation of the specific energy dissipation rate ϵ, in particular. Also, the range of variations in the sizes of the surfaces was limited. The present analysis is based on a turbulent velocity field generated by direct integration of the Navier-Stokes equation in a periodic box of size $L=2\pi$. The integration is carried out by means of pseudospectral codes with resolutions 512^3 and 1024^3, respectively, for the two cases. Energy is injected into the flow by keeping the total energy in each of the two first wave number shells constant. The flow motions are damped by a second-order viscous dissipation term. Passive tracer trajectories are obtained by integrating $d\mathbf{x}(t)/dt=\mathbf{u}[\mathbf{x}(t),t]$ with the velocity at the instantaneous particle positions, obtained by linear interpolation from the nearest grid points. More details on the simulations can be found on the site [21]. The relation between computational and physical units was discussed elsewhere [13]. The number of full length particle trajectories available are 192×10^3 and 384×10^3 for data set *A* and *B*, respectively. For

TABLE I. Simulation A (second column) lasts 1167 time steps with $dt=0.005$, simulation B (third column) lasts 1841 time steps with $dt=0.0023$. The Kolmogorov length scale is here η and the specific energy dissipation is ϵ, while τ_η is the Kolmogorov time scale. The Reynolds number is Re_λ, while T is the duration of the simulation in computational time units [3].

dx	$2\pi/512=0.012272$	$2\pi/1024=0.0061359$
ν	2.05×10^{-3}	8.8×10^{-4}
ϵ	0.8853212	0.810878
$E=\frac{1}{2}\langle u^2\rangle$	3.01	2.96
Re_λ	183	286
η	$0.00993=0.81\ dx$	$0.0054=0.88\ dx$
τ_η	0.048	0.033
T	5.84	4.23

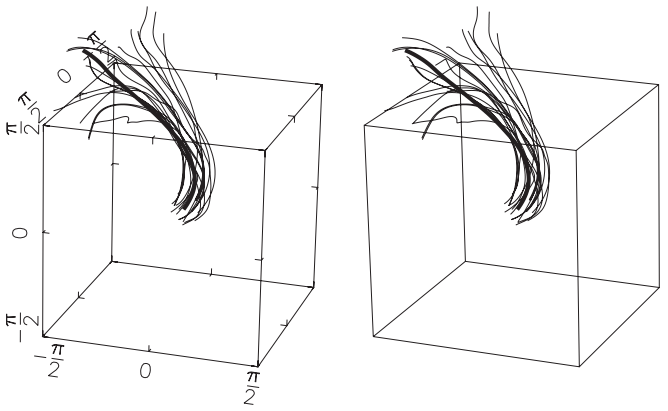

FIG. 1. Trajectories of selected point particles in the Eulerian or rest frame. The particles are initially confined to a sphere of radius $R=0.2$. The figure allows a three-dimensional, stereoscopic view. Units on axes are in computational units. The heavy line shows the reference particle. The figure is representative for R being in the inertial subrange. For comparison, we have the scale size of the largest energy containing eddies to be ~ 3 in the present computational units.

the analysis, these trajectories are broken up into two shorter segments. With the available numerical database, we can improve the accuracy of previous estimates considerably and also extend the parameter ranges to length scales shorter than the Kolmogorov scale.

The complexity of the problem can be illustrated by Figs. 1 and 2 showing trajectories of selected point particles followed in the simulations. In the case of a sphere fixed in the Eulerian frame, the transit time can be obtained approximately by assigning all particles one characteristic velocity determined by the largest energy containing eddies in the system [11]. The *same* particles followed in the Lagrangian frame of the reference particle give a much more complicated presentation of the orbits, see Fig. 2. This latter case corresponds to the problem addressed in the present work. All trajectories refer to the same time interval (here 600 time steps), and their relative lengths are thus representative for an average velocity associated with each of the corresponding

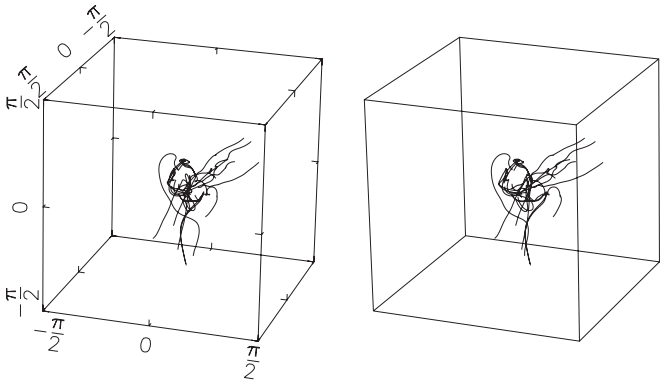

FIG. 2. Trajectories of the point particles in Fig. 1 now shown in the Lagrangian or comoving frame for the particle in the center. The reference particle is represented by a point in this comoving frame, and therefore not noticeable.

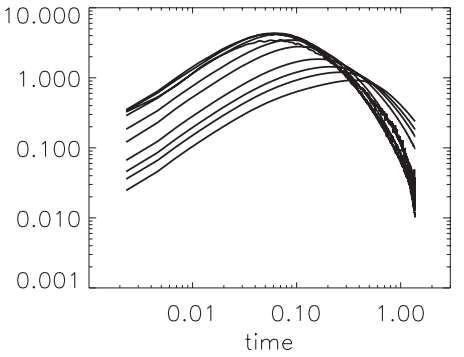

FIG. 3. Transit time distribution as a function of computational times for the spherical case, for radii $R=0.025$, 0.050, 0.075, 0.100, 0.175, 0.25, 0.50, 0.75, 1.00, and 1.50. The top curves to the left correspond to the smallest R value, with increasing R giving steadily decreasing functional values there. The results are for the data set with $\mathrm{Re}_\lambda=286$. Times are in computational units, see Table I.

trajectories. The figures shown here are only illustrative: they can appear very different from one realization to another.

Figures 1 and 2 allow a three-dimensional, stereoscopic view by focusing the eyes approximately 20 cm behind the plane of the paper or computer screen. It requires a little exercise. In our experience, the distance to the eyes is not so critical provided it is sufficiently large, but it is essential that the figure is kept plane and horizontally aligned with the observer's eyes. A similar type of presentation of curves in three dimensions was used in several presentations [14], where many examples are found.

II. NUMERICAL RESULTS FOR THE INERTIAL SUBRANGE

In Fig. 3, we show the distribution of transit times to spheres of different radii, covering the inertial as well as the viscous subranges. These results are obtained by use of data set B in Table I. We note a systematic variation, finding in particular that the curves collapse (the curves fall on top of each other) when the radii are smaller than a critical length $\eta_0=\eta\sqrt{15C_K}$ separating the inertial and viscous subranges, with $C_K\approx 2.1$ being the Kolmogorov constant. This critical length η_0 is approximately a factor 13 larger than the Kolmogorov length scale [15]. The characteristic length-scale η_0 is obtained by identifying a transition length between the structure functions for the inertial subrange, $C_K(\epsilon r)^{2/3}$, and the viscous subrange, $r^2(\epsilon/\nu)/15$, respectively [16]. Equating the two structure functions, we obtain the crossover length-scale η_0 separating them [15]. For data set A, we have $\eta_0\approx 0.13$, and for B, we have $\eta_0\approx 0.07$ in normalized computational units. Structure functions obtained for the two simulations are shown elsewhere [13,15].

In the inertial subrange of the turbulence, where the effect of viscosity ν on the structure function is negligible, we expect that a universal scaling law should exist depending only on t, ϵ and R. This scaling can be determined by dimensional reasoning [7,17,18]. First, we consider the spherical case, with a given radius R. We need a universal "time" for nor-

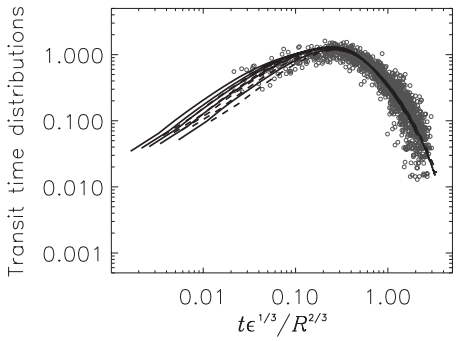

FIG. 4. Normalized transit time distributions for the spherical case with radii $R=0.25$, 0.5, 0.75, 1.0, and 1.5, all in the inertial subrange for both data sets with $\mathrm{Re}_\lambda=183$ and 286 given with dashed and full lines, respectively. With gray circles, we also shown normalized results obtained from a laboratory experiment [11], for six values of ϵ, each analyzed for 4 radii in the inertial subrange. No free parameters are involved in the comparison of numerical and experimental results.

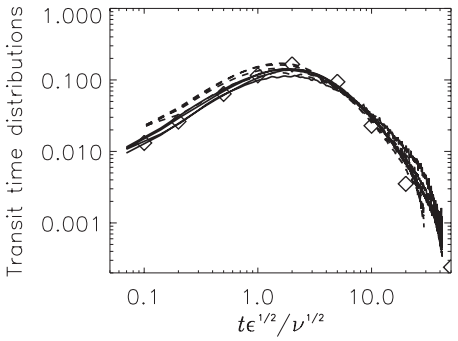

FIG. 5. Normalized transit time distributions for the spherical case with radii $R=0.025$, 0.050, 0.075, and 0.100, all in the viscous subrange. Results from both data sets are included here, and shown with full and dashed lines. Diamonds give analytical results for selected points using the simple model (2).

malization, and with the parameters ϵ and R being the only dimensional parameters available, the only characteristic time available is $R^{2/3}/\epsilon^{1/3}$. In the inertial length interval, we thus expect that the probability density for the occupation times can be written in terms of a dimensionless temporal variable as $P(t)=(R^{2/3}/\epsilon^{1/3})P_L(t\epsilon^{1/3}/R^{2/3})$, assuming that ϵ is a deterministic constant being the same for all surfaces in a given simulation. In reality, ϵ is fluctuating around the average value, and the corrections due to these intermittency effects are ignored. We have P_L to be a dimensionless function of a dimensionless variable. The form of the function P_L cannot be determined by dimensional reasoning. It will depend in particular on the shape of the reference volume.

In Fig. 4, we show results of the normalized transit time distributions in terms of normalized times. Superposed on this figure, we have the similar results for different parameter values, as obtained by a laboratory experiment [11]. There are no free fitting parameters for this comparison of results. To obtain the results shown in Fig. 3, we follow 20×10^3 moving particles with their associated volumes in time. We find very good agreement between the laboratory results and those obtained in the present numerical analysis.

For large transit times, we find that the proposed scaling laws are very well satisfied, while the agreement deteriorates somewhat for smaller transit times. These shorter times are, however, in general associated with "glancing" transitions, where the length of the particle orbit between the entrance and exit positions will often be much shorter than η_0, and therefore a scaling law derived for the inertial subrange is unlikely to hold there. Another factor contributing to the uncertainty is that transit times are measured in units of integer sampling times (see caption of Table I), which becomes problematic for very small transit times. When the Reynolds number is very large (i.e., much larger than achieved by the present simulations), the relative importance of these short transit distances will become small and a better agreement with the proposed scaling can be expected, although intermittency effects may become noticeable in this limit. The agreement between the results from simulations and laboratory experiment is fully satisfactory, indicating that the estimation of the energy dissipation ϵ was successful in that experiment: this is in general difficult. In particular we argue that this agreement demonstrates that the inertial subrange of the turbulence was fully developed in that experiment [12]. We find that the overall features (although not all details) of the transit time probability density for spherical volumes can be adequately represented by a Rayleigh distribution, $(x/\sigma^2)\exp(-\frac{1}{2}(x/\sigma)^2)$, with $x\equiv t\epsilon^{1/3}/R^{2/3}$ and $\sigma\approx1/3$. This approximation can be useful for modeling.

III. NUMERICAL RESULTS FOR THE VISCOUS SUBRANGE

The scaling laws for the viscous subrange are different from those characterizing the inertial subrange. From Fig. 3, we thus note that when $R<\eta_0$ all curves seem to collapse. The only normalizing quantity with dimension "time" being independent of R is $\sqrt{\nu/\epsilon}$. In Fig. 5, we show the transit time distribution as function of normalized time $t\sqrt{\epsilon/\nu}$, for a range of R values, and the two values of the kinematic viscosity available. For the smallest R values, we have relatively few events contributing, and the signal-to-noise level is correspondingly reduced. For this viscous subrange, we do not have any laboratory experimental data points available. The general agreement with the proposed scaling is just as good in Fig. 5 as in Fig. 4.

IV. NONSPHERICAL VOLUMES

The general form of the scaling laws derived by dimensional arguments is not restricted to spherical surfaces of interception. The only assumption is, in fact, that the entire volume changes self-similarly with a change in a characteristic length scale. The scaling law should therefore apply equally well to a hemisphere, for instance, but with a different form of the function P_L. In Fig. 6, we show results of transit times for a hemisphere, where the radii are in the inertial subrange for both data sets in Table I. Again we find the scaling for the normalized temporal variable to be well fulfilled, that is the curves for different R, ϵ, and ν collapse

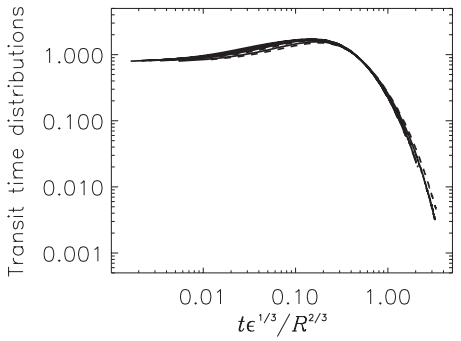

FIG. 6. Numerically obtained normalized transit time probability densities for R in the inertial subrange and $\theta=90°$. See also Fig. 7. We have $R=0.25$, 0.5, 0.75, 1.0, and 1.5. Full and dashed lines are for the two cases listed in Table I.

on each other. The orientation of the symmetry axes of the hemispheres are randomly distributed with respect to the local flow vector directions. If we consider the case of microorganisms following the flow, this assumption seems the only one reasonable, since these organisms will have limited means to detect the magnitude of the local flow velocity or its direction. Also, more complicated surfaces of interception can be relevant for the biological applications mentioned [19], but the hemispherical case discussed here has received attention in several studies [20].

In Fig. 7, we show results of transit times for a hemisphere in terms of the normalized time $t\sqrt{\epsilon/\nu}$, where the radii are in the viscous subrange, $R<\eta_0$. We use both data sets, thus having two different values of ν. We find that the scaling law is well satisfied also here. Again we find only few simulation particles with separations smaller than 0.05, so the curves for the smallest values of R have a noticeable noise component. Superposed the curves from the data analysis, we show analytical results by diamonds as in Fig. 5.

Comparing transit time distributions for spherical and hemispherical volumes, we note that for the hemisphere the probability of long transit times is reduced and thus short time probabilities are increased. This follows naturally from the reduction in volume available for accommodating the trajectories.

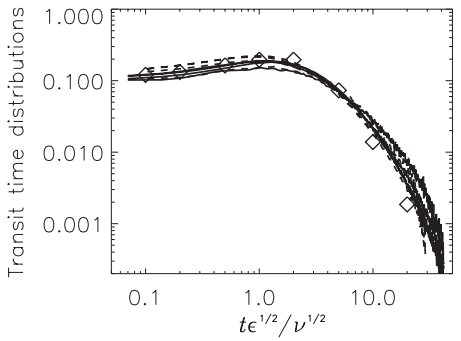

FIG. 7. Numerically obtained normalized transit time probability densities for R in the viscous subrange and $\theta=90°$. Full and dashed lines are for the two cases listed in Table I. We have $R=0.025$, 0.05, 0.075, and 0.1. The curves with $R=0.1$ are the bottom ones to the left/outer ones to the right. Diamonds give analytical results for selected points using a simple shear-flow model.

V. SIMPLE SOLVABLE MODELS

Based on results from numerical flow simulations, we have obtained estimates for the transit time distributions of point particles moving with the flow. The analysis covers parameter ranges where length scales for the surfaces are in the inertial as well as the viscous subranges of the turbulence [16]. Data from two independent numerical solutions of the Navier-Stokes equation demonstrated a very good agreement with the proposed scalings.

Transit time distributions were studied before [7,11] using data from a laboratory experiment, although those studies were restricted to the inertial subrange of the turbulence. For comparison, we show also these experimental results in Fig. 4. We found a very good agreement, noting in particular that there are no free parameters to fit. We were thereby also able to make an independent test of the calibration of the estimates of the average specific energy dissipation rate ϵ in that experiment [12].

The independence of the transit time distribution of the scale length R in the viscous range might appear surprising, but the result can be illustrated by physically realizable local flow models having precisely this property. For scales smaller than the Kolmogorov length, we can argue that viscosity will damp out all variations except locally linear shears. For illustration, we therefore consider a simple linear velocity shear profile $\mathbf{U}=\{\alpha z,0,0\}$ in the comoving frame of reference. For those passages that give short transit times, we expect this simple model to be adequate also physically.

The transit time distribution of a cube $L\times L\times L$, with axes parallel to the x,y,z axes, is readily found as $P(t)=1/(\alpha t^2)$ for $t\geq 1/\alpha$ and $P(t)=0$ otherwise. This result is independent of the scale size of the box, here L, consistent with our observations for the case where the scale sizes are smaller than η_0.

We can also obtain a simple analytical result for transit times of a spherical surface for the previous simple linear shear-flow profile. Consider particles propagating in the x-direction, with the coordinates x,y,z being distributed on the "back" surface of the sphere with radius R. We have $R^2=x^2+y^2+z^2$. The transit time of a particle is $t=2x/\alpha z=(2/\alpha z)\sqrt{R^2-y^2-z^2}$. For a given time t, the locus of such particles is then $y^2+(1+(\alpha t/2)^2)z^2=R^2$. The flux of particles at a position $\{x,y,z\}$ is given by the product of a velocity αz and a constant density, irrespective of x and y. The cumulative distribution $F(t)$ of transit times for given R is then obtained as

$$F(t)=C_1 2\int_0^R \int_{\sqrt{R^2-y^2}/\sqrt{1+(\alpha t/2)^2}}^{\sqrt{R^2-y^2}} \alpha z dz dy$$
$$=C_1\alpha\frac{(\alpha t/2)^2}{1+(\alpha t/2)^2}\int_0^R (R^2-y^2)dy=C_2\frac{(\alpha t/2)^2}{1+(\alpha t/2)^2}, \quad (1)$$

with constants determined by the requirement $F(t\to\infty)\to 1$. In particular, we find $C_2=1$. The probability density $P(t|\alpha)$ for transit times in the present simple model with given α is then found as

$$P(t|\alpha) = \frac{dF(t)}{dt} = \alpha \frac{\alpha t/2}{(1+(\alpha t/2)^2)^2}, \tag{2}$$

which has its maximum for $\alpha t = 2/\sqrt{3}$. As a consequence of the assumed linear velocity shear, the result (2) is also independent of the radius R of the reference sphere. The shear parameter is directly related to the magnitude of the vorticity, $|\boldsymbol{\omega}| = \alpha$, of the given shear flow. If the probability density of ω is known, we can obtain the transit time distribution for $R < \eta_0$. Being restricted to simple shear flows, the present outline does not generally *prove* P to be independent of R when $R < \eta_0$, but it makes the observed result plausible.

It can have some interest to compare the analytical result (2) with the numerically obtained transit time distribution. For this purpose, we inserted selected values as indicated by diamonds, $\diamond$, in Fig. 5, where we fitted the maximum at $t\sqrt{\epsilon/\nu} \approx 2.25$ to the maximum of Eq. (2), which gives $\alpha \approx 2/(2.25\sqrt{3})\sqrt{\epsilon/\nu} \approx 0.5\sqrt{\epsilon/\nu}$. In the model (2), we have α entering as a free parameter, but we can approximate $\alpha^2 \approx \langle(\nabla \mathbf{u})^2\rangle = \int_0^\infty k^2 E(k) dk$ in terms of the velocity power spectrum $E(k)$. We have $\epsilon = \nu \int_0^\infty k^2 E(k) dk$ implying $\alpha = \sqrt{\epsilon/\nu}$, which is within a factor 2 the result we found before. Given the simplifying assumptions made to obtain this result for the viscous subrange, we find the agreement to be good.

For spherical volumes with radii in the viscous subrange, the present analysis supports a universal form for the transit time probability density

$$P_{4\pi}(t) \simeq \frac{1}{8} \frac{t\epsilon/\nu}{\left(1 + \frac{1}{16} t^2 \epsilon/\nu\right)^2}, \tag{3}$$

where the subscript 4π refers to the spherical surface.

The analytical result reproduces the numerically obtained transit time distribution very well for most transit times, except for the largest ones where we find the probability density to have a negative curvature, indicating that it falls off exponentially rather than the power law t^{-3} given by Eq. (2). The simple analytical model studied here evidently applies only for short transit times. Large transit times will in general be associated with long convoluted trajectories that cannot easily be modeled. This conclusion applies for R being in the inertial as well as the viscous subranges. Even the simple shear model studied before will become very complicated for large transit times, where α can no longer be considered constant in time. We find that using a Rayleigh model for the probability density in the viscous range transit times we can account for the variation observed at large times, and at the same time also for the short time behavior of Eq. (3).

Superposed the curves in Fig. 7, we show our analytical results by diamonds as in Fig. 5. We use again the previous simple shear-flow model, but let the reference volume be a hemisphere with a symmetry axis being randomly distributed with respect to the flow. The analysis becomes rather lengthy for this problem, so we show here only the final result obtained numerically, where we averaged over all angles between the local flow velocity vector and the symmetry axis of the hemisphere, assuming these angles to be uniformly distributed over 4π. When inserting the analytical result, we use the same value for α as in Fig. 5, so there are no new parameters introduced. Again we find a good agreement at short transit times, while we again find indications of an exponential fall-off at large transit times not accounted for by the simple model. An important point is that the difference between the transit time distributions for the spherical and hemispherical reference volumes can be explained by this simple model, i.e., in the spherical case we have for the probability density the limit $P_{4\pi}(t \to 0) = 0$, while for the hemispherical case, we find $P_{2\pi}(t \to 0) > 0$, where the subscript specifies the opening angle of the cone defining the volume. Also other shapes of the reference volume have been analyzed. A simple analytical model is here found only for the viscous subrange where the simple shear-flow $\mathbf{U} = \{\alpha z, 0, 0\}$ is unaffected by the viscosity term $\nu \nabla^2 \mathbf{u}$ in Navier-Stokes equation. In the inertial subrange, the trajectories will be strongly convoluted (see Fig. 2), and the analysis is significantly more complicated. Results for this inertial subrange are, however, reported in the literature [1]. These results are supported by numerical results based on a Langevin equation. A nontrivial scatter at small transit times was found, so the agreement with our numerical results for the inertial subrange is not evident.

The normalizing time for the transit times can also be argued on dimensional grounds by taking it to be the ratio of the characteristic length R and a typical velocity estimated by the root-mean-square of the second-order Eulerian structure function, corresponding to the same length scale. For the *inertial* subrange, this argument gives $R/(\epsilon R)^{1/3} = R^{2/3}/\epsilon^{1/3}$, in agreement with the previous result. This normalizing time $R^{2/3}/\epsilon^{1/3}$ was argued also in the literature [1], but as we see it is the only one that can be made dimensionally correct with the given set of parameters for the inertial subrange.

With the second-order structure function being $r^2(\epsilon/\nu)/15$ in the *viscous* subrange [16], the previous arguments give (apart from a numerical constant) the characteristic time for transit time normalizations as $R/\sqrt{R^2\epsilon/\nu} = \sqrt{\nu/\epsilon}$ as before, independent of R in this limit.

For R in the inertial as well as the viscous subrange, our results favor a decay of the probability density faster than any t^{-p} for large transit times, for instance, an exponential variation. Analytical results [1] seem to argue for a $t^{-5/2}$ in the transit time probability density for large times with R in the inertial subrange. (This result implies that $\langle t^p \rangle$ should not exists for any $p \geq 3/2$.) As stated, our observations are in variance with this result.

VI. CONCLUSIONS

We studied particle transit times through given reference surfaces. The particles are assumed to be carried passively by turbulent motions in the environment. We demonstrated the applicability of some simple scaling laws for the probability densities of the appropriate statistical distributions for the inertial as well as the viscous subranges. We also illustrated the relations between the present numerical results and existing laboratory studies of the same problem, obtaining a good agreement for spherical surfaces.

The results summarized in the present work have relevance for cases where interaction times are important. We

already mentioned the relevance for micro-organisms in turbulent environments, but relevance also for chemical reaction rates have been noted [1]. Information concerning the net rate of interactions needs the additional information of the encounter rates [5,6], which have been studied previously, experimentally as well as numerically [7,15]. This latter problem has relevance for several applications like those mentioned.

We studied the Lagrangian version of the transit time problem because only this is relevant for the applications outlined here, but it has evidently also an Eulerian counterpart [7,11]. For studies of aquatic micro-organisms, the Eulerian problem has little relevance, but it can be interesting for other cases. Since the particle trajectories are much smoother in the Eulerian frame (see Fig. 1), we expect that simple models can be obtained for this case using a characteristic velocity to be $\sqrt{\langle u^2 \rangle}$, as argued elsewhere [7,11].

Intermittency effects in the inertial as well as the viscous subranges were, as already mentioned, not considered when obtaining the scaling arguments by dimensional reasoning. The good agreement with the proposed scaling seems to indicate that intermittency effects have a minor role for the present problem, at least for the Reynolds numbers in the present simulations. Intermittency effects could be expected to be particularly important for the smallest scales of the analysis, but this was not observed. We expect that observation of intermittency effects in the present context requires Reynolds numbers significantly exceeding those available here.

ACKNOWLEDGMENTS

We thank Guido Boffetta for helping us to access the database from the numerical simulations, and for his interest and comments. The supercomputing center Cineca (Bologna, Italy) is acknowledged for hosting the data [21]. Valuable discussions with Jacob Berg Jørgensen, Jakob Mann, and Søren Ott are gratefully acknowledged. The authors were in part supported by the "Effects of North Atlantic Climate Variability on the Barents Sea Ecosystem" (ECOBE) project.

[1] S. Pigolotti, M. H. Jensen, and A. Vulpiani, Phys. Fluids **18**, 048104 (2006).
[2] L. Biferale, G. Boffetta, A. Celani, B. J. Devenish, A. Lanotte, and F. Toschi, Phys. Rev. Lett. **93**, 064502 (2004).
[3] L. Biferale, G. Boffetta, A. Celani, A. Lanotte, and F. Toschi, Phys. Fluids **17**, 021701 (2005).
[4] T. Kiørboe, *A Mechanistic Approach to Plankton Ecology* (Princeton University Press, USA, 2008).
[5] B. J. Rothschild and T. R. Osborn, J. Plankton Res. **10**, 465 (1988).
[6] T. Osborn, J. Plankton Res. **18**, 185 (1996).
[7] J. Mann, S. Ott, H. L. Pécseli, and J. Trulsen, Phys. Rev. E **67**, 056307 (2003).
[8] Ø. Fiksen and B. R. MacKenzie, Mar. Ecol.: Prog. Ser. **243**, 151 (2002).
[9] D. M. Lewis and T. J. Pedley, J. Theor. Biol. **210**, 347 (2001).
[10] G. Boffetta and I. M. Sokolov, Phys. Fluids **14**, 3224 (2002).
[11] J. Berg Jørgensen, J. Mann, S. Ott, H. L. Pécseli, and J. Trulsen, Phys. Fluids **17**, 035111 (2005).
[12] S. Ott and J. Mann, J. Fluid Mech. **422**, 207 (2000).
[13] G. Boffetta, H. L. Pécseli, and J. Trulsen, J. Turbul. **7**(22), 1 (2006).
[14] P. M. Morse and H. Feshbach, *Methods of Theoretical Physics*, International Series in Pure and Applied Physics (McGraw-Hill, New York, 1953).
[15] H. L. Pécseli and J. Trulsen, J. Turbul. **8**(42), 1 (2007).
[16] P. A. Davidson, *Turbulence. An Introduction for Scientists and Engineers* (Oxford University Press, UK, 2004).
[17] J. Mann, S. Ott, H. L. Pécseli, and J. Trulsen, Phys. Rev. E **65**, 026304 (2002).
[18] E. Buckingham, Phys. Rev. **4**, 345 (1914).
[19] D. M. Lewis and S. I. Bala, J. Theor. Biol. **242**, 44 (2006).
[20] D. M. Lewis, J. Theor. Biol. **222**, 73 (2003).
[21] The data can be freely downloaded from the web address http://cfd.cineca.it/. Conditions for usage are given at http://cfd.cineca.it/cfd/repository/folder.2006-01-20.4761556357/document.2006-01-20.5299514280/